but instead, S–C bonds were broken and S atoms became the bridges. Similarly, in the previous preparations of the last three compounds in Table VI, sulfur atoms were completely removed from the sulfur reagents employed. In the case of $Ta_2(\mu\text{-}S)_2Cl_4(EtSCH_2CH_2SEt)_2$ the source of the μ-S atoms might have been either the Me_2S ligands in the starting material, $Ta_2Cl_6(SMe_2)_3$, or the $EtSCH_2CH_2SEt_2$. For the two $M_2(\mu\text{-}S)_2Cl_4(SMe_2)_4$ compounds, the source might have been either MeSSMe or Me_2S. There has recently been a report showing directly that S can be abstracted from Me_2S in the reaction of a diphosphine with $Ta_2Cl_6(SMe_2)_3$.[16]

A question clearly arises as to why the reaction of $Nb_2Cl_6(SMe_2)_3$ with $EtSCH_2CH_2SEt$ did not lead to a compuond with μ-S groups, as in the case of the tantalum analogue. The answer is that it probably did, but not as a major product. As noted in ref 4, it was thought that in addition to the main form of $Nb_2Cl_6(EtSCH_2CH_2SEt)_2$, for which the structure was there reported, a second form was obtained in small amounts. It was shown to have a unit cell nearly identical with that of what we now recognize to be one form of $Ta_2(\mu\text{-}S)_2Cl_4(EtSCH_2CH_2SEt)_2$. We have now obtained, and described here, an authentic second form of this compound.

The observation that both $M^{III}_2(\mu\text{-}Cl)_2$ and $M^{IV}_2(\mu\text{-}S)_2$ products can be formed in the same reaction is in accord with another observation we have made. When the preparation[4,17] of "$Ta_2Cl_6(EtSCH_2CH_2SEt)_2$" was carried out on a fairly large scale, the product gave a microanalysis inconsistent with either the $(\mu\text{-}Cl)_2$ or the $(\mu\text{-}S)_2$ product, but indicative of a mixture of both. Evidently the process of transferring sulfur from an organosulfur molecule to the bridge positions in the dinuclear complex proceeds at different relative rates for different cases. There is also the question of which product crystallizes most readily if both are present.

It is clear that considerable work will have to be done to discover how to obtain either the $M^{III}_2(\mu\text{-}Cl)_2$ or the $M^{IV}_2(\mu\text{-}S)_2$ product in any given system cleanly, in good yield, and with certainty beforehand as to which it will be. Whether Clay and Brown,[17] who used $M_2Cl_6(c\text{-}C_4H_8S)_3$ as starting material, really obtained $M_2Cl_6(EtSCH_2CH_2SEt)_2$ products as they presumed is uncertain. Our repetition of one of their preparations gave a mixture according to the elemental analysis. One might suppose that tetrahydrothiophene would be more resistant to sulfur abstraction than SMe_2, but $Et_2SCH_2CH_2SEt_2$ must also be considered as a sulfur source in these reactions.

Acknowledgment. We thank Dr. W. A. Herrmann for his assistance in the microanalysis performed at the Technical University of Munich. We thank the Robert A. Welch Foundation (Grant No. A-494) for support.

Supplementary Material Available: For both compounds, tables listing full crystallographic data, bond distances and angles, and anisotropic thermal parameters (13 pages); tables of calculated and observed structure factors (25 pages). Ordering information is given on any current masthead page.

(16) Fryzuk, M. D.; McConville, D. H. *Inorg. Chem.* **1989**, *28*, 1613.
(17) Clay, M. E.; Brown, T. M. *Inorg. Chim. Acta* **1983**, *72*, 75.

Contribution from the Department of Chemistry, Faculty of Science, Osaka City University, Osaka 558, Japan

The Dinuclear Palladium(II) Complex of Pyridine-2-thiol. Synthesis, Structure, and Electrochemistry

Keisuke Umakoshi,[1] Akio Ichimura, Isamu Kinoshita, and Shun'ichiro Ooi*

Received May 24, 1989

Reaction of pyridine-2-thiol (pytH) with $Pd_3(CH_3COO)_6$ gives $[Pd_2(pyt)_4]$ (**1**), but that with $PdCl_2(CH_3CN)_2$ gives $[Pd(pytH)_4]Cl_2$ (**2**), the alkalization of which yields **1**. Reaction of **1** with iodine yields neither a dinuclear $Pd^{II}Pd^{III}$ nor $Pd^{III}Pd^{III}$ complex but tetranuclear $[Pd_4I_2(pyt)_6]$ (**3**). The structures **1**–**3** have been investigated by X-ray crystallography. Two Pd atoms in **1** are bridged by four pyt ligands in such way that two *cis*-PdS_2N_2 units centrosymmetrically face each other. The Pd···Pd distance is 2.677 (1) Å. The cation of **2** has a square-planar coordination by four S atoms. All pyridine N atoms are protonated and linked to chloride ions by N–H···Cl hydrogen bonds. The tetranuclear complex **3** has C_2 symmetry. Four Pd atoms are disposed in a rhombic configuration and bridged by the pyt ligands, diagonal Pd···Pd distances being 3.009 (2) and 7.024 (6) Å. There are two kinds of Pd coordination spheres: PdS_3N and *trans*-$PdIsN_2$. Cyclic voltammetry showed that $[Pd_2(pyt)_4]$ undergoes an irreversible one-electron oxidation (E_{pa} = 0.61 V vs Ag/Ag^+) in CH_2Cl_2 containing only TBAP as a supporting electrolyte. In the presence of halide ion, however, the compound undergoes a quasi-reversible two-electron oxidation at much more lower potential ($E_{1/2}$ = 0.13 V for Cl^- and 0.15 V for Br^-) with the uptake of one halide ion. These electrochemical results indicate that one electron per Pd atom is removed from the metal-based MO. Crystal data: $[Pd_2(pyt)_4]\cdot 2CHCl_3$, monoclinic, space group $P2_1/c$, a = 12.518 (2) Å, b = 6.587 (1) Å, c = 18.878 (3) Å, β = 99.09 (1)°, Z = 2; $[Pd(pytH)_4]Cl_2$, triclinic, space group $P\bar{1}$, a = 9.006 (2) Å, b = 10.059 (3) Å, c = 8.329 (2) Å, α = 115.17 (2)°, β = 75.03 (2)°, γ = 113.09 (2)°, Z = 1; $[Pd_4(pyt)_6I_2]\cdot C_3H_7NO$, monoclinic, space group $P2/c$, a = 14.335 (9) Å, b = 9.030 (2) Å, c = 17.401 (9) Å, β = 108.30 (8)°, Z = 4.

Introduction

In contrast to the many dinuclear Pt^{III}_2 complexes with d^7–d^7 bonds reported in the last decade, no corresponding Pd^{III}_2 complex has been synthesized as yet. The Pd^{III} oxidation state is unusual but is stabilized by appropriate donor atoms as demonstrated by the isolation of some mononuclear Pd^{III} complexes.[2] Several dinuclear complexes of the $[Pd(bridge)_4Pd]$ type have been synthesized and structurally characterized,[3-7] some of which have been electrochemically investigated in order to probe the generation of $[Pd^{III}(bridge)_4Pd^{III}]^{n+}$ complexes. Cotton and co-workers isolated an intriguing complex, $[Pd_2(form)_4]PF_6$ (form = $(p\text{-}CH_3C_6H_4)NCHN(p\text{-}CH_3C_6H_4)^-$), but concluded that both Pd atoms in this seemingly $Pd^{II}Pd^{III}$ dimer are divalent and the odd electron occupies a ligand-based MO,[3] whereas Bear and coworkers detected $[Pd^{II}(\mu\text{-dpb})_4Pd^{III}]^+$ (dpb = *N*,*N*′-diphenylbenzamidinate) in the electrolyzed solution of $[Pd(\mu\text{-dpb})_4Pd]$.[7]

(1) Present address: Department of Chemistry, Faculty of Science, Naruto University of Education, Naruto, Tokushima 772, Japan.
(2) (a) Blake, A. J.; Holder, A. J.; Hyde, T. I.; Schröder, M. *J. Chem. Soc., Chem. Commun.* **1987**, 987–988. (b) McAuley, A.; Whitcombe, T. W. *Inorg. Chem.* **1988**, *27*, 3090–3099.
(3) (a) Cotton, F. A.; Matusz, M.; Poli, R.; Feng, X. *J. Am. Chem. Soc.* **1988**, *110*, 1144–1154. (b) Cotton, F. A.; Matusz, M.; Poli, R. *Inorg. Chem.* **1987**, *26*, 1472–1474.
(4) Clegg, W.; Garner, C. D.; Al-Samman, M. H. *Inorg. Chem.* **1982**, *21*, 1897–1901.
(5) Bancroft, D. P.; Cotton, F. A.; Falvello, L. R.; Schwotzer, W. *Inorg. Chem.* **1986**, *25*, 1015–1021.
(6) Piovesana, O.; Bellitto, C.; Flamini, A.; Zanazzi, P. F. *Inorg. Chem.* **1979**, *18*, 2258–2265.
(7) Yao, C.-L.; He, L.-P.; Korp, J. D.; Bear, J. L. *Inorg. Chem.* **1988**, *27*, 4389–4395.

0020-1669/90/1329-4005$02.50/0

Table I. Crystallographic Data for X-ray Diffraction Studies

	$[Pd_2(pyt)_4]\cdot 2CHCl_3$	$[Pd(pytH)_4]Cl_2$	$[Pd_4I_2(pyt)_6]\cdot C_3H_7NO$
formula	$C_{22}H_{18}Cl_6N_4Pd_2S_4$	$C_{20}H_{20}Cl_2N_4PdS_4$	$C_{33}H_{31}I_2N_7OPd_4S_6$
cryst syst	monoclinic	triclinic	monoclinic
space group	$P2_1/c$	$P\bar{1}$	$P2/c$
a/Å	12.518 (2)	9.006 (2)	14.335 (9)
b/Å	6.587 (1)	10.059 (3)	9.030 (2)
c/Å	18.878 (3)	8.329 (2)	17.401 (9)
α/deg		115.17 (2)	
β/deg	99.09 (1)	75.03 (2)	108.30 (8)
γ/deg		113.09 (2)	
V/Å^3	1537.2 (2)	624.4 (3)	2139 (2)
Z	2	1	2
d_{calcd}/(g/cm^3)	1.93	1.66	2.20
cryst size/mm	0.11 × 0.62 × 0.06	0.20 × 0.25 × 0.10	0.31 × 0.18 × 0.01
data collecn instrument	Philips PW1100	Rigaku AFC-5	Rigaku AFC-5
scan range/deg	1.2 + 0.4 tan θ	1.2 + 0.5 tan θ	1.2 + 0.4 tan θ
scan mode	ω	ω–2θ	ω–2θ
scan speed/(deg s^{-1})	0.033	0.05	0.133
bkgd estimation at each end of the scan/s	10	8	4
$2\theta_{max}$/deg	46.0	55.0	60.0
μ(Mo Kα)/cm^{-1}	19.5	12.9	34.0
octants collected	$\pm h,+k,+l$	$\pm h,\pm k,+l$	$\pm h,+k,+l$
no. of unique rflns	2130	3086	6637
no. of obsd rflns with $F_o > 3\sigma(F_o)$	1495	2431	2612
$R = \sum\|\|F_o\| - \|F_c\|\|/\sum\|F_o\|$	0.043	0.029	0.052
$R_w = [\sum w(\|F_o\| - \|F_c\|)^2/\sum w\|F_o\|^2]^{1/2}$	0.050	0.035	0.037

We have conducted the syntheses of the dinuclear Pt^{II}_2 complexes of pyridine-2-thiol (pytH) and its analogue in order to convert them into the corresponding Pt^{III}_2 complexes by oxidation.[8,9] An attempt has also been made to synthesize the Pd^{III}_2 complex by oxidation of $[Pd_2(pyt)_4]$.[10] The electrochemical investigation of $[Pt_2(pyt)_4]$ in the presence of halide ion (X^-) revealed that $[Pt_2(pyt)_4]^{2+}$ generated by oxidation immediately coordinates halide ions, giving $[Pt_2X_2(pyt)_4]$, which reverts back to $[Pt_2(pyt)_4]$, releasing halide ions upon reduction; i.e. $[Pt_2(pyt)_4]$ in the presence of twice as many moles of X^- shows a cyclic voltammogram essentially identical with that of $[Pt_2X_2(pyt)_4]$.[8] Such an electrochemical investigation may be useful to examine the formation of the Pd^{III}_2 complex, provided that it requires the presence of X ligands as its Pt^{III}_2 analogue does. In this paper we describe the synthesis, structure, and electrochemical properties of $[Pd_2(pyt)_4]$ in detail, along with the product of the $[Pd_2(pyt)_4]$ reaction with iodine as well as $[Pd(pytH)_4]Cl_2$, which serves as the starting material for the dimer.

Experimental Section

Materials. $Pd_3(CH_3COO)_6$ and pyridine-2-thiol (pytH) were purchased from Wako Pure Chemical Industries, Ltd., and pyridine-2-thiol was recrystallized from benzene for use. Dichloromethane was dried over 4-Å molecular sieves and distilled under an argon atmosphere. *N*,*N*-Dimethylformamide (DMF) was dried over 3-Å molecular sieves and anhydrous copper sulfate and then distilled twice under reduced pressure. Tetrabutylammonium perchlorate (TBAP) and tetrabutylammonium bromide were recrystallized twice from ethanol and ethyl acetate, respectively. Tetrabutylammonium chloride was purified by a literature method.[11] All salts were dried at 60 °C under vacuum before use.

$[Pd_2(pyt)_4]$ (1). (a) From $Pd_3(CH_3COO)_6$. A mixture of $Pd_3(CH_3COO)_6$ (673 mg, 1 mmol) and pyridine-2-thiol (667 mg, 6 mmol) was stirred in dioxane (150 cm^3) for 15 min at room temperature. A brown solid initially precipitated, which then dissolved to give a red solution. An orange solid, which appeared after a few minutes, was washed with dioxane and ethanol and dried in vacuo; yield 940 mg (96%). Recrystallization from chloroform gave the orange crystals of $[Pd_2(pyt)_4]\cdot 2CHCl_3$, the formula of which was confirmed by X-ray structure analysis. The crystals were pulverized gradually on standing by loss of chloroform, and therefore the solvent of crystallization was completely removed in vacuo prior to chemical analysis. Anal. Calcd for $C_{10}H_8N_2PdS_2$: C, 36.76; H, 2.47; N, 8.58. Found: C, 36.85; H, 2.46; N, 8.42.

(b) From $[Pd(pytH)_4]Cl_2$ (2). An aqueous solution of $Pd(pytH)_4]Cl_2$ (622 mg, 1 mmol/100 cm^3) was alkalized by 1 N KOH(aq) (30 cm^3). An orange solid separated out when the solution was kept at 90 °C for 10 min on a hot plate. The product was washed with water and dried in vacuo; yield 293 mg (90%). It was recrystallized from chloroform.

$[Pd(pytH)_4]Cl_2$ (2). $[PdCl_2(CH_3CN)_2]$ (260 mg, 1 mmol) and pyridine-2-thiol (445 mg, 4 mmol) were refluxed in dioxane (50 cm^3) for 12 h. The orange-yellow precipitate was filtered out, washed with dioxane and ethanol, and dried in vacuo; yield 480 mg (77%). Recrystallization from water gave orange crystals of $[Pd(pytH)_4]Cl_2$. Anal. Calcd for $C_{20}H_{20}Cl_2N_4PdS_4$: C, 38.61; H, 3.25; N, 9.01. Found: C, 38.85; H, 3.25; N, 9.10.

$[Pd_4(pyt)_6I_2]$ (3). To a chloroform suspension of $[Pd_2(pyt)_4]$ (327 mg, 0.5 mmol/150 cm^3) was added a chloroform solution of a 0.5-equivalent amount of iodine (63 mg, 0.25 mmol/30 cm^3) with stirring. The resulting red solution was evaporated to dryness. A 50-mL quantity of ether was added to the residue, and the mixture was stirred for a few minutes. The ether layer was separated off, and the remaining solid was recrystallized from DMF/ether; yield 337 mg. Anal. Calcd for $C_{33}H_{31}I_2N_7OPd_4S_6$: C, 28.04; H, 2.21; N, 6.94. Found: C, 28.47; H, 2.33; N, 7.19.

A 52-mg sample of pale yellow oil was obtained by evaporation of the ether layer. It was crystallized from ligroin and identified with authentic bis(2-pyridyl) disulfide:[12] ^{1}H NMR ($CDCl_3$) δ 7.11 (ddd; J = 6.71, 4.88, 1.83 Hz; 2 H), 7.59–7.64 (m, 4 H), 8.47 (d, J = 4.88 Hz; 2 H); IR (neat) 1572 (s), 1561 (s), 1447 (s), 1418 (s), 1278 (m), 1148 (m), 1114 (s), 1085 (m), 1043 (m), 987 (m), 758 (s), 718 (m), 617 (m) cm^{-1}. Anal. Calcd for $C_{10}H_8N_2S_2$: C, 54.51; H, 3.67; N, 12.72. Found: C, 54.44; H, 3.65; N, 12.69. The yields of **3** and bis(2-pyridyl) disulfide were 95% in the synthetic reaction, $2[Pd_2(pyt)_4] + I_2 \rightarrow [Pd_4(pyt)_6I_2]$ + bis(2-pyridyl) disulfide.

X-ray Structural Studies. Weissenberg photographs taken with Cu Kα radiation were used for investigating Laue symmetry, space group, and approximate unit-cell dimensions. Since $[Pd_2(pyt)_4]\cdot 2CHCl_3$ (**1**·$2CHCl_3$) and $[Pd_4(pyt)_6I_2]\cdot C_3H_7NO$ (**3**·C_3H_7NO) are decomposed by loss of solvent of crystallization, they were sealed in a thin-walled glass capillaries for use. The accurate cell dimensions for **1**·$2CHCl_3$, **2**, and **3**·C_3H_7NO were determined from the least-squares treatment of 36 ($12 \le 2\theta \le 26°$), 50 ($22 \le 2\theta \le 32°$), and 21 ($19 \le 2\theta \le 30°$) reflections, respectively, measured on a diffractometer by use of Mo Kα radiation (λ = 0.71069 Å) at 295 ± 2 K (Table I). Intensities were measured on the diffractometer using graphite-monochromated Mo Kα radiation. The intensities of three standard reflections (500, 020, 008 for **1**·$2CHCl_3$; 400, 020, 001 for **2**; 500, 050, 008 for **3**·C_3H_7NO), monitored every 4 h, showed no appreciable decay during the data collection. Absorption

(8) Umakoshi, K.; Kinoshita, I.; Ichimura, A.; Ooi, S. *Inorg. Chem.* **1987**, *26*, 3551–3556.
(9) Umakoshi, K.; Kinoshita, I.; Fukui-Yasuba, Y.; Matsumoto, K.; Ooi, S.; Nakai, H.; Shiro, M. *J. Chem. Soc., Dalton Trans.* **1989**, 815–819.
(10) Umakoshi, K.; Kinoshita, I.; Ooi, S. *Inorg. Chim. Acta* **1987**, *127*, L41–L42.
(11) Unni, A. K. R.; Elias, L.; Schiff, H. I. *J. Phys. Chem.* **1963**, *67*, 1216–1219.
(12) Marckwald, W.; Klemm, W.; Trabert, H. *Chem. Ber.* **1900**, *33*, 1556.

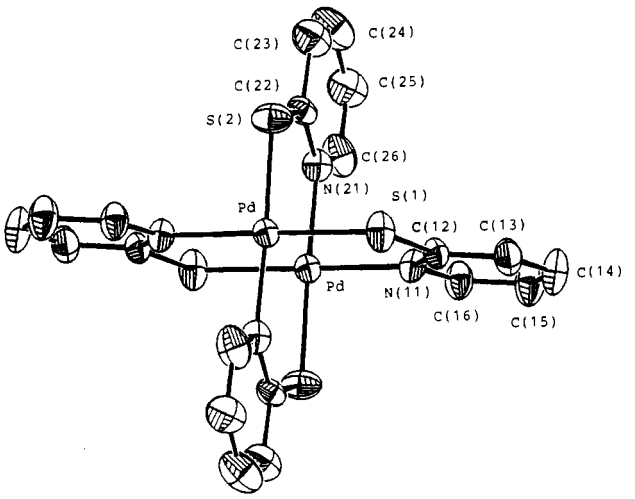

Figure 1. ORTEP diagram of $[Pd_2(pyt)_4]$ (50% probability contours for all atoms).

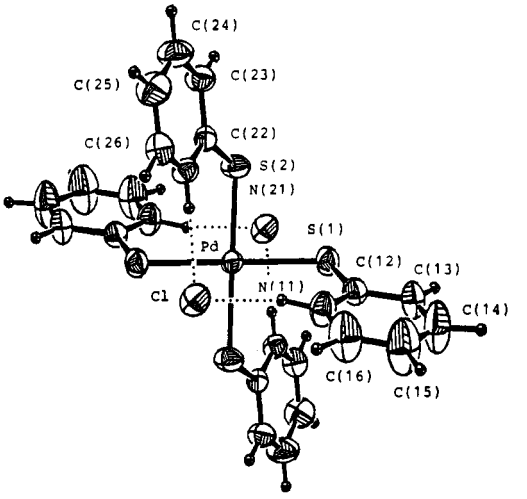

Figure 2. ORTEP diagram of $[Pd(pytH)_4]Cl_2$. Thermal ellipsoids are drawn at the 50% probability level. Hydrogen atoms are represented by spheres with arbitrary radii. Dotted lines indicate N–H···Cl hydrogen bonds.

correction was made for $3\cdot C_3H_7NO$[13] but not for $1\cdot 2CHCl_3$ and **2**.

The crystal structures were solved by the Patterson–Fourier method. The positional and thermal parameters were refined by the block-diagonal-matrix least-squares method. The minimized function was $\sum w(|F_o| - |F_c|)^2$, where $w^{-1} = \sigma^2(|F_o|)$ for $1\cdot 2CHCl_3$ and $3\cdot C_3H_7NO$ and $w^{-1} = \sigma^2(|F_o|) + (0.015|F_o|)^2$ for **2**. All hydrogen atoms were located in the calculated positions with isotropic temperature factors and included in the refinement of **2**. The convergence was attained with the R and R_w given in Table I.[14] The dimethylformamide molecule in $3\cdot C_3H_7NO$ was found to be disordered about the crystallographic 2-fold axis, and so the structure refinement was conducted by using a model in which the N and C(CO) atoms were fixed on the 2-fold axis. In the final cycle of the refinement, parameter shifts were less than 0.1σ except for those in the disordered dimethylformamide molecule, for which $\Delta_{max}/\sigma = 0.71$. No correction was made for secondary extinction. No attempt was made to locate hydrogen atoms in the structure analysis for $1\cdot 2CHCl_3$ and $3\cdot C_3H_7NO$. The atomic scattering factors, with correction for anomalous dispersion of Pd^0, Cl^0, and S were taken from ref 16. Computational work was carried out by using ORFLS,[15] ORTEP,[17] and standard programs in UNICS.[18]

Electrochemical Measurements. Cyclic voltammetry was performed with a Yanaco P-1100 system equipped with a Rika Denki RW-201K X-Y recorder. The working and the counter electrodes were a glassy-carbon disk and a platinum wire. Cyclic voltammograms were recorded in CH_2Cl_2 at a scan rate of 50 mV/s unless otherwise stated. Two kinds of reference electrodes were used: Ag/Ag^+ for CH_2Cl_2 and $Ag/Ag(Cryp(2,2))^+$ (Cryp(2,2) = cryptand(2,2))[19] for DMF. The reference electrodes were checked periodically against the ferrocenium/ferrocene couple (Fc^+/Fc) in CH_2Cl_2 and in DMF, respectively. The half-wave potentials of Fc^+/Fc ($E_{1/2}(Fc^{+/0})$ vs Ag/Ag^+ and vs $Ag/Ag(cryp(2,2))^+$) were +0.205 and +0.466 V, respectively.

Controlled-potential coulometry was carried out in 0.1 M TBAP–CH_2Cl_2 with a standard H-type cell with a Hokuto HA-501 potentiostat and a Hokuto HF-201 coulometer. The working electrode was reticulated vitreous carbon, and the working compartment was separated from the counter compartment by a sintered-glass disk.

Electrochemical measurements were performed at 25 ± 1 °C. The sample solutions (ca. 0.2 mM) containing 0.05 or 0.1 M TBAP as supporting electrolyte were deoxygenated with a stream of argon. All potentials reported here are relative to the Ag/Ag^+ reference electrode unless otherwise stated.

Measurements. The ^1H NMR spectra were obtained at 400 MHz with a JEOL GX-400 spectrometer. ^1H chemical shifts were measured relative to the methyl resonance of TMS. UV–visible spectra were recorded on a Hitachi 330 spectrophotometer at room temperature.

Results and Discussion

Structure. Figure 1 shows the X-ray structure of **1**, which is structurally similar to $[Pt_2(4\text{-mpyt})_4]$ (4-mpyt = 4-methylpyridine-2-thiolate).[8] There is an inversion center at the midpoint of Pd···Pd contact, and accordingly the molecule has an approximate symmetry of C_{2h}. The square-planar PdS_2N_2 coordination sphere has a cis configuration. The two spheres are disposed in the eclipsed conformation, the S–Pd···Pd–N torsion angles being less than 2° (Table II). The $Pd^{II}\cdots Pd^{II}$ distance (2.677 (1) Å) is comparable to that in $[Pd_2(form)_4]$ (2.622 (3) Å)[3] but significantly longer than those in $[Pd_2(mhp)_4]$ (2.546 (1)–2.559 (3) Å, mhp = 6-methyl-2-hydroxypyridinate),[4,5] $[Pd_2(chp)_4]$ (2.567 (2) Å, chp = 6-chloro-2-hydroxypyridinate),[5] and $[Pd_2(\mu\text{-dpb})_4]$ (2.576 (1) Å)[7] and shorter than those in $[Pd_2(CH_3CS_2)_4]$ (2.754 (1), 2.738 (1) Å).[6] The Pd atom lies in the S_2N_2 coordination plane, the deviation from which is 0.027 (3) Å.

Part of the crystal structure of **2** is shown in Figure 2. The Pd atom lies on inversion center and has a square-planar coordination by four S atoms. The Cl anions are located above and below the coordination plane at distances of 3.380 (1) Å from the Pd atom. The Pd→Cl vector intersects the coordination plane at 69.24 (3)°. All protons linked to the pyridine N atoms participate in N–H···Cl^- hydrogen bonding. The [S(1), N(11), ···, C(16)] and [S(2), N(21), ···, C(26)] planes make angles of 64.8 (3) and 64.2 (1)° with the coordination plane. The Pd–S distance is 0.04 Å longer than that in **1**. The mean value of C–S distances (1.713 Å) is 0.03 Å shorter than those of **1** and its Pt analogue.[8] These facts indicate that the pytH ligand has a greater contribution from the following resonance structure:

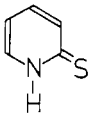

A decrease of negative charge on the S atom in comparison with that in the pyt ligand may be responsible for an elongation of the Pd–S bond.

The X-ray structure analysis disclosed that $3\cdot C_3H_7NO$ is formulated as $[Pd_4I_2(pyt)_6]\cdot C_3H_7NO$. The tetramer (Figure 3) has a 2-fold axis perpendicular to the Pd(1)···Pd(1′) axis. Four Pd atoms are disposed in a rhombic configuration, Pd(1)···Pd(1′) and Pd(2)···Pd(2′) being 3.009 (2) and 7.024 (6) Å, respectively. Every Pd atom is divalent and has an essentially planar coordination. There are two kinds of Pd coordination spheres: PdS_3N and *trans*-$PdISN_2$. The two types of the pyt ligands differ in the

(13) Crystal faces: 100, $\bar{1}00$, 011, $0\bar{1}\bar{1}$, $01\bar{1}$, $0\bar{1}1$, 001, $00\bar{1}$. $\Delta d(100\text{–}\bar{1}00) = 0.010$ mm, $\Delta d(011\text{–}0\bar{1}\bar{1}) = 0.31$ mm, $\Delta d(01\bar{1}\text{–}0\bar{1}1) = 0.31$ mm, and $\Delta d(001\text{–}00\bar{1}) = 0.18$ mm. Transmission factor range: 0.61–0.97.
(14) Structure refinement of $3\cdot C_3H_7NO$ based on the space group *Pc* gave a very distorted dimethylformamide structure without significant improvement in the *R* value.
(15) Busing, W. R.; Martin, K. O.; Levy, H. A. ORFLS. Report ORNL-TM-305; Oak Ridge National Laboratory: Oak Ridge, TN.
(16) *International Tables for X-ray Crystallography*; Kynoch Press: Birmingham, England, 1974; Vol. IV.
(17) Johnson, C. K. ORTEP II. Report ORNL-5138: Oak Ridge National Laboratory: Oak Ridge, TN, 1976.
(18) UNICS, Crystallographic Society of Japan, 1969.
(19) Izutsu, K.; Ito, M.; Sarai, E. *Anal. Sci.* **1985**, *1*, 341–344.

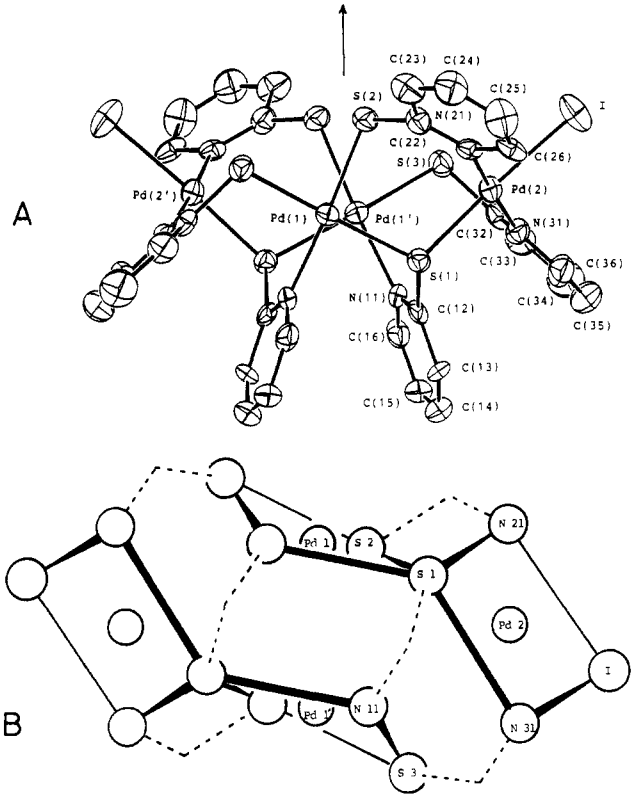

Figure 3. (A) ORTEP diagram of $[Pd_4I_2(pyt)_6]$, showing 50% probability ellipsoids. The arrow indicates the 2-fold axis. (B) Disposition of Pd^{II} coordination spheres in $[Pd_4I_2(pyt)_6]$ viewed down the 2-fold axis. Dashed lines represent the pyt ligands.

ligation mode of S atom. The S(1) atom directly bridges Pd(1) and Pd(2), whereas S(2) and S(3) are linked to separate Pd atoms. The mean $Pd-S_{bridge}$ distance (2.339 Å) is somewhat longer than the mean distance of Pd–S(2) and Pd–S(3) (2.314 Å), although the difference between the two mean values is not significant on statistical grounds. Bond lengths, bond angles, and some of the torsion angles are summarized in Table II. Atomic coordinates of **1**·2$CHCl_3$, **2**, and **3**·C_3H_7NO are listed in Table III.

$[Pt_2(pyt)_4]$ was obtained in high yield by the reaction of *cis*-$[PtCl_2(NH_3)_2]$ with the pytH in dioxane.[8] Therefore, we initially tried to synthesize the Pd analogue by the reaction of $[PdCl_2(CH_3CN)_2]$ with pytH in dioxane, but the reaction did not afford any dinuclear complex but **2**. It was thereafter found that the alkalization of **2** in water yields **1**: the single crystals obtained by recrystallization of the product from chloroform have the same unit-cell dimensions as those of **1**·2$CHCl_3$. The reaction is formally represented as

$$2[Pd(pytH)_4]Cl_2 + 8KOH \rightarrow [Pd_2(pyt)_4] + 4KCl + 4pytK + 8H_2O$$

An $[M(A-B)_4M]$ type of complex, where A and B denote different kinds of donor atoms, exists in the four isomers. The Pd^{II} complex is known to be labile for ligand substitution reactions and hence for isomerization, and accordingly it is difficult to isolate isomers other than the most stable one. Selective formation of *cis*-$[Pd_2(pyt)_4]$, irrespective of synthetic path, indicates that it is the most stable isomer among the four ("cis" and "trans" are used to denote the isomers that have *cis*-PdS_2N_2 and *trans*-PdS_2N_2 halves, respectively). Cotton and co-workers, however, found that the unit cell of $[Pd_2(mhp)_4]_5$·6$CHCl_3$ comprises the cis and trans isomers in a ratio of 1:4.[5] In $[Pd_2(chp)_4]$ and $[Pd_2(mhp)_4]$ the trans isomer seems to be more stable than the cis isomer, since the syntheses of these complexes selectively gave the trans isomer except for the case of $[Pd_2(mhp)_4]_5$·6$CHCl_3$.[5] Steric repulsion between the substituents at the 6-position of the pyridine rings may be responsible for the selective formation of one isomer, since the intersubstituent distance is shorter in the cis isomer than in the trans one.

Table II. Selected Bond Distances and Angles of $[Pd_2(pyt)_4]$·2$CHCl_3$ (**1**), $[Pd(pytH)_4]Cl_2$ (**2**), and $[Pd_4I_2(pyt)_6]$·C_3H_7NO (**3**)

	1	2	3
	Bond Distances (Å)		
Pd(1)···Pd(1′)	2.677 (1)		3.009 (2)
Pd(1)···Pd(2)			3.818 (4)
Pd(1′)···Pd(2)			3.891 (3)
Pd(1)–N(11)	2.077 (7)		
Pd(1)–N(21′)	2.072 (7)		
Pd(1)–S(1)		2.335 (1)	2.343 (4)
Pd(1)–S(1′)	2.293 (3)		
Pd(1)–S(2)	2.292 (2)	2.336 (1)	2.306 (4)
Pd(2)–I			2.617 (2)
Pd(1)···Cl		3.380 (1)	
Pd(2)–N(21)			2.024 (9)
Pd(2)–N(31)			2.039 (9)
Pd(2)–S(1)			2.335 (3)
Pd(1′)–N(11′)	2.077 (7)		
Pd(1′)–N(11)			2.108 (9)
Pd(1′)–N(21)	2.072 (7)		
Pd(1′)–S(1)	2.293 (3)		
Pd(1′)–S(2′)	2.292 (2)		
Pd(1′)–S(3)			2.321 (4)
C(12)–S(1)	1.750 (9)	1.714 (3)	1.773 (12)
C(22)–S(2)	1.737 (9)	1.712 (3)	1.760 (13)
C(32)–S(3)			1.767 (11)
N(11)···Cl		3.062 (3)	
N(21)···Cl		3.086 (3)	
	Bond Angles (deg)		
N(11)–Pd(1)–N(21′)	88.2 (3)		
N(11)–Pd(1)–S(2)	89.9 (2)		
S(1′)–Pd(1)–N(21′)	90.6 (2)		
S(1′)–Pd(1)–S(2)	91.3 (1)		
S(1)–Pd(1)–S(2)		88.33 (4)	94.4 (1)
N(21)–Pd(2)–S(1)			88.0 (3)
N(31)–Pd(2)–S(1)			93.7 (3)
I–Pd(2)–S(1)			175.3 (1)
I–Pd(2)–N(31)			87.6 (2)
N(21)–Pd(2)–I			90.3 (2)
N(11)–Pd(1′)–S(3)			94.4 (2)
Pd(1)–N(11)–C(12)	124.3 (6)		
Pd(2)–N(21)–C(22)	122.7 (6)		
Pd(1)–S(1)–Pd(2)			109.4 (1)
Pd(1)–S(1)–C(12)		110.1 (1)	109.0 (4)
Pd(2)–S(1)–C(12)			107.8 (3)
Pd(1′)–S(1)–C(12)	110.9 (3)		
Pd(1)–S(2)–C(22)	111.6 (3)	109.9 (1)	106.1 (4)
Pd(1′)–S(3)–C(32)			106.2 (4)
N(11)–Cl–N(21)		96.2 (1)	
	Torsion Angles (deg)		
S(1)–Pd(1′)–Pd(1)–N(11)	1.1 (2)		
S(1)–Pd(1)–Pd(1′)–N(11)			35.0 (3)
N(21)–Pd(1′)–Pd(1)–S(2)	1.9 (2)		
Pd(1)–S(1)–C(12)–N(11)		−5.0 (3)	
Pd(1)–S(2)–C(22)–N(21)		3.1 (3)	

$[Pt^{II}_2(L)_4]$ (L = pyt or 4-mpyt) abstracts the Cl atom from chloroform to give $[Pt^{III}_2Cl_2(L)_4]$[8] and reacts with iodine to quantitatively give $[Pt_2I_2(L)_4]$.[20] The $Pt(L)_4Pt$ core remains unchanged in these oxidation reactions. However, the Pd analogue does not react with chloroform and the reaction with iodine does not yield any Pd^{III} species but affords the tetranuclear Pd^{II} complex: $2[Pd_2(pyt)_4] + I_2 \rightarrow [Pd_4I_2(pyt)_6]$ + bis(2-pyridyl) disulfide.

The UV–visible absorption spectrum of $[Pd_2(pyt)_4]$ is shown in Figure 4. While the divalent dinuclear platinum complex, $[Pt_2(pyt)_4]$, is yellow and has no absorption peak in the visible region, $[Pd_2(pyt)_4]$ is orange and shows an absorption maximum at 430 nm (ϵ = 2150). The peak of this type is absent in the mononuclear complex, $[Pd(pytH)_4]Cl_2$; such an absorption seems to be characteristic of $[Pd^{II}(bridge)_4Pd^{II}]$ type complexes, since similar absorptions are also found in $[Pd_2(mhp)_4]$ (ca. 370 nm, ϵ = 2200),[4] $[Pd_2(CH_3CSS)_4]$ (397 nm, ϵ = 2290),[6] $[Pd_2(form)_4]$

(20) Kinoshita, I.; Umakoshi, K.; Matsumoto, K.; Ooi, S. To be published.

Table III. Positional Parameters and Isotropic Temperature Factors[a]

atom	x	y	z	B_{eq}, Å^2	atom	x	y	z	B_{eq}, Å^2
				A. $[Pd_2(pyt)_4]\cdot 2CHCl_3$					
Pd	0.9735 (1)	0.3150 (1)	0.52088 (4)	2.09 (1)	C(23)	0.8388 (8)	0.460 (2)	0.2804 (5)	4.2 (3)
N(11)	0.8344 (5)	0.421 (1)	0.5556 (4)	2.3 (2)	C(24)	0.842 (1)	0.623 (2)	0.2355 (5)	4.7 (4)
C(12)	0.7993 (7)	0.616 (1)	0.5485 (4)	2.4 (2)	C(25)	0.8993 (9)	0.799 (2)	0.2591 (6)	4.5 (3)
C(13)	0.6999 (7)	0.674 (2)	0.5696 (5)	3.6 (3)	C(26)	0.9505 (8)	0.808 (2)	0.3295 (5)	4.0 (3)
C(14)	0.6394 (8)	0.532 (2)	0.5989 (6)	4.1 (3)	S(2)	0.8784 (2)	0.2703 (4)	0.4079 (1)	3.4 (1)
C(15)	0.6782 (8)	0.330 (2)	0.6070 (6)	4.1 (3)	C	0.6468 (9)	0.958 (2)	0.3686 (6)	5.8 (4)
C(16)	0.7747 (7)	0.283 (1)	0.5846 (5)	3.1 (3)	Cl(1)	0.6230 (3)	0.6906 (7)	0.3678 (2)	8.1 (1)
S(1)	0.8721 (2)	0.8099 (4)	0.5143 (1)	3.2 (1)	Cl(2)	0.5774 (3)	1.0642 (7)	0.4320 (2)	8.2 (1)
N(21)	0.9461 (6)	0.648 (1)	0.3753 (4)	2.7 (2)	Cl(3)	0.5976 (5)	1.055 (1)	0.2853 (3)	14.7 (3)
C(22)	0.8909 (7)	0.478 (1)	0.3532 (4)	2.4 (2)					
				B. $[Pd(pytH)_4]Cl_2$					
Pd	0.0	0.0	0.0	2.85 (1)	C(24)	−0.4446 (4)	−0.1166 (5)	0.5895 (5)	5.3 (1)
Cl	−0.2886 (1)	−0.3459 (1)	−0.1635 (1)	4.19 (2)	C(25)	−0.5385 (4)	−0.2386 (4)	0.4556 (5)	5.2 (1)
S(1)	0.2196 (1)	−0.0641 (1)	0.0090 (1)	3.99 (3)	C(26)	−0.4794 (4)	−0.2604 (4)	0.2845 (5)	4.2 (1)
S(2)	−0.0506 (1)	0.0709 (1)	0.3098 (1)	3.99 (3)	H(N11)	−0.040 (5)	−0.315 (5)	−0.149 (5)	7.8 (11)
N(11)	0.0484 (3)	−0.3585 (3)	−0.1752 (4)	4.5 (1)	H(C13)	0.412 (4)	−0.248 (4)	−0.081 (4)	4.7 (8)
C(12)	0.1876 (3)	−0.2587 (3)	−0.1050 (4)	3.8 (1)	H(C14)	0.375 (5)	−0.517 (4)	−0.232 (5)	7.4 (11)
C(13)	0.3111 (4)	−0.3204 (4)	−0.1305 (5)	5.1 (1)	H(C15)	0.128 (5)	−0.680 (5)	−0.369 (6)	8.8 (12)
C(14)	0.2881 (5)	−0.4743 (5)	−0.2249 (8)	8.2 (2)	H(C16)	−0.085 (5)	−0.576 (4)	−0.314 (5)	6.7 (10)
C(15)	0.1423 (6)	−0.5724 (5)	−0.2969 (8)	9.0 (2)	H(N21)	−0.297 (4)	−0.186 (3)	0.128 (4)	3.6 (7)
C(16)	0.0247 (5)	−0.5117 (5)	−0.2686 (7)	7.3 (2)	H(C23)	−0.235 (4)	0.054 (4)	0.629 (4)	4.5 (7)
N(21)	−0.3328 (3)	−0.1658 (3)	0.2422 (3)	3.4 (1)	H(C24)	−0.486 (4)	−0.100 (4)	0.711 (5)	5.6 (9)
C(22)	−0.2370 (3)	−0.0459 (3)	0.3656 (4)	3.3 (1)	H(C25)	−0.642 (4)	−0.304 (4)	0.484 (4)	5.0 (8)
C(23)	−0.2974 (4)	−0.0241 (4)	0.5439 (4)	4.1 (1)	H(C26)	−0.540 (4)	−0.342 (4)	0.188 (4)	4.7 (8)
				C. $[Pd_4(pyt)_6I_2]\cdot C_3H_7NO$[a]					
Pd(1)	0.0093 (1)	0.8379 (1)	0.1662 (1)	2.25 (3)	C(23)	0.197 (1)	0.525 (1)	0.1072 (7)	4.1 (5)
Pd(2)	0.2576 (1)	0.7811 (1)	0.3282 (1)	2.46 (3)	C(24)	0.287 (1)	0.523 (2)	0.0952 (8)	4.7 (5)
I	0.3868 (1)	0.5944 (1)	0.4165 (1)	4.52 (3)	C(25)	0.3636 (9)	0.601 (2)	0.1461 (7)	4.6 (5)
S(1)	0.1527 (2)	0.9558 (4)	0.2458 (2)	2.4 (1)	C(26)	0.3529 (8)	0.679 (1)	0.2127 (7)	3.0 (4)
S(2)	0.0740 (2)	0.6027 (4)	0.1927 (2)	3.1 (1)	N(31)	0.2640 (6)	0.889 (1)	0.4327 (5)	2.7 (3)
S(3)	0.1109 (2)	0.7204 (4)	0.4372 (2)	2.9 (1)	C(32)	0.2043 (8)	0.853 (1)	0.4768 (6)	2.7 (4)
N(11)	0.0612 (6)	1.046 (1)	0.3540 (5)	2.7 (3)	C(33)	0.215 (1)	0.913 (1)	0.5521 (7)	4.4 (5)
C(12)	0.1213 (8)	1.086 (1)	0.3097 (6)	2.6 (4)	C(34)	0.289 (1)	1.011 (2)	0.5825 (8)	5.7 (6)
C(13)	0.1590 (8)	1.235 (1)	0.3147 (7)	3.3 (4)	C(35)	0.351 (1)	1.057 (2)	0.5346 (8)	5.1 (5)
C(14)	0.1346 (9)	1.332 (1)	0.3671 (7)	4.2 (5)	C(36)	0.3357 (9)	0.988 (1)	0.4612 (7)	4.3 (5)
C(15)	0.0736 (9)	1.286 (1)	0.4133 (7)	4.0 (5)	SC(1)[a]	0.452 (2)	0.250 (3)	0.295 (1)	19 (1)
C(16)	0.0377 (8)	1.141 (1)	0.4064 (6)	3.3 (4)	SN[a]	0.5	0.171 (3)	0.25	12.4 (8)
N(21)	0.2638 (6)	0.679 (1)	0.2263 (5)	2.4 (3)	SC(2)[a]	0.5	0.015 (4)	0.25	14 (1)
C(22)	0.1872 (8)	0.607 (1)	0.1733 (6)	2.9 (4)	SO[a]	0.470 (2)	−0.028 (3)	0.287 (1)	11.1 (8)

[a] SC(1), SC(2), SN, and SO denote the methyl and carbonyl carbons, nitrogen, and oxygen atoms of the dimethylformamide molecule. These atoms were refined isotropically, occupancy factor of 0.5 being assigned to the SN, SC(2), and SO.

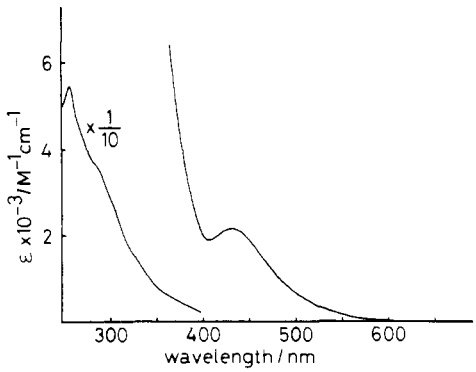

Figure 4. Absorption spectrum of $[Pd_2(pyt)_4]$ in chloroform.

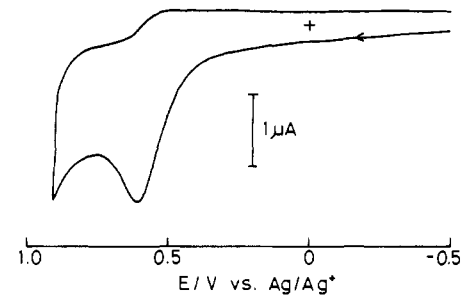

Figure 5. Cyclic voltammogram of $[Pd_2(pyt)_4]$ in 0.1 M TBAP–CH_2Cl_2 at a glassy-carbon electrode with a scan rate of 50 mV/s.

(492 nm, ϵ = 2600),[3] and $[Pd_2(\mu\text{-dpb})_4]$ (500 nm, ϵ = 2500).[7]

Electrochemistry. $[Pd_2(pyt)_4]$ exhibits an irreversible oxidation wave (v = 50 mV/s) with E_{pa} = 0.763 V vs Ag/Ag(Cryp(2,2))$^+$ in 0.05 M TBAP–DMF ($E_{1/2}(Fc^{+/0})$ = 0.466 V), while $[Pt_2(pyt)_4]$ exhibits an electrochemically quasi-reversible two-electron oxidation process with $E_{1/2}$ = 0.282 V under the same condition;[8] i.e. the peak potential of $[Pd_2(pyt)_4]$ for oxidation is 0.5 V more positive than that of the platinum analogue. As CH_2Cl_2 is more favorable for measuring the oxidation process than DMF, we have used CH_2Cl_2 as solvent in all the other electrochemical measurements of the Pd complex. Figure 5 shows the cyclic voltammogram of **1** in CH_2Cl_2 at a glassy-carbon electrode. As in DMF, **1** exhibits an irreversible oxidation peak with E_{pa} = 0.608 V in 0.1 M TBAP–CH_2Cl_2, wherein $E_{1/2}(Fc^{+/0})$ = 0.205 V. Bulk controlled-potential coulometry at 0.75 V with a reticulated vitreous carbon electrode in CH_2Cl_2 reveals that the oxidation is a one-electron process. The electrolyzed solution showed no wave in the +0.9 to −0.5 V range. The irreversible behavior, even at −50 °C with a scan rate of 500 mV/s, indicates a rapid decomposition of the one-electron-oxidation product $[Pd_2(pyt)_4]^+$.

Addition of halide ion (Cl^- or Br^-) to the electrolytic solution gives a new redox couple at much more negative potential. In the case of iodide and thiocyanate, their oxidation obscured the oxidation process of $[Pd_2(pyt)_4]$. Figure 6 illustrates the cyclic voltammogram of $[Pd_2(pyt)_4]$ in the presence of chloride and bromide ions. $[Pd_2(pyt)_4]$ shows a quasi-reversible oxidation wave with $E_{1/2}$ = 0.129 V for Cl^- and 0.150 V for Br^-; the slight difference in $E_{1/2}$ is ascribed to the difference in stabilization of

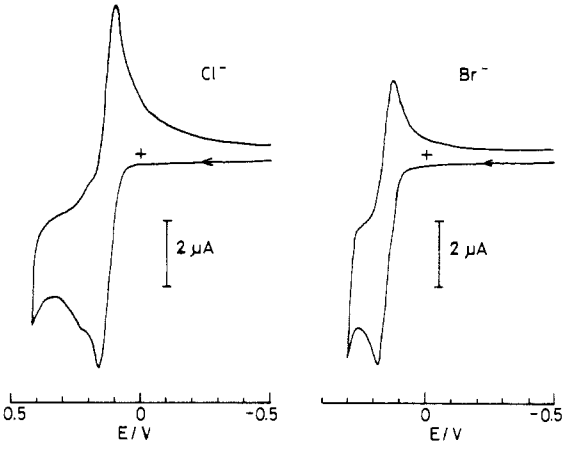

Figure 6. Cyclic voltammograms of $[Pd_2(pyt)_4]$ in the presence of 0.01 M Bu_4NCl (left) and 0.01 M Bu_4NBr (right) in 0.1 M TBAP–CH_2Cl_2 at a glassy-carbon electrode with a scan rate of 50 mV/s.

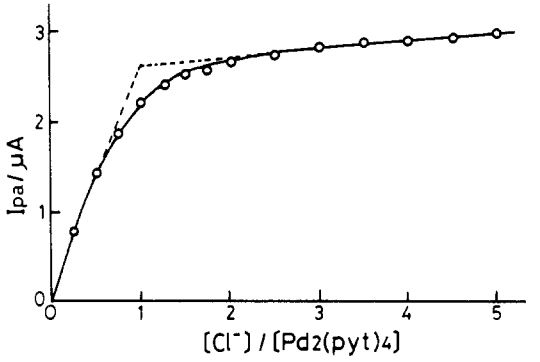

Figure 7. Plot of the anodic peak current for $[Pd_2(pyt)_4]$ against the chloride ion/$[Pd_2(pyt)_4]$ mole ratio.

the oxidation product by halide ion. In the chloride solution a further small redox couple appears at 0.22 V, which is more positive than the potential of the main redox couple. The oxidation peak current for the main redox couple is proportional to the square root of the scan rate within 20–400 mV/s. This observation indicates that the oxidation process is diffusion-controlled. The anodic and cathodic peak separations (ΔE_p) are 59 mV for Cl^- and 56 mV for Br^-.[21] The ΔE_p value for ferrocene exhibiting a reversible one-electron oxidation process in CH_2Cl_2 is 95 mV under the same conditions, which is larger than the theoretical value of 59 mV because of the large solution resistance in CH_2Cl_2. Thus, the oxidation of $[Pd_2(pyt)_4]$ is a quasi-reversible two-electron process.[22] The ratio of cathodic to anodic peak currents, which is a measure of the stability of the oxidation product, is 1.00 for Cl^- and 0.66 for Br^- at v = 50 mV/s, indicating that the oxidation product in chloride solution is more stable than that in bromide solution. As shown in Figure 7, the oxidation peak current at 0.16 V linearly increases with the increase of chloride ion concentration until the mole ratio $[Cl^-]/[Pd_2(pyt)_4]$ reaches 1.0 and then remains almost constant beyond this value. Thus, $[Pd_2(pyt)_4]$ takes up one halide ion in the course of the oxidation process:

$$[Pd_2(pyt)_4] + X^- \rightleftharpoons [Pd_2(pyt)_4X]^+ + 2e^-$$

Good reversibility of the cyclic voltammetric behavior is indicative of the retention of the $Pd(pyt)_4Pd$ core during the electrode process. Presumably, X^- is coordinate at, and released from, the axial coordination site of $[Pd_2(pyt)_4]^{2+}$, as is the case for $[Pt_2(pyt)_4]^{2+}$.

As described above, X^- has a large influence on the oxidation potential of $[Pd_2(pyt)_4]$, giving a large negative peak potential shift (~0.5 V): i.e. the oxidation takes place much more easily in the presence of an X^- ion. The electron release probably occurs from the metal-based MO, as in the case of $[Pt_2(pyt)_4]$, which releases two electrons from the $d\sigma^*$ orbital, yielding $[XPt(pyt)_4PtX]$.

Bulk controlled-potential coulometry of $[Pd_2(pyt)_4]$ at 0.35 V in the presence of the Cl^- ion gave the number of electrons transferred as 1.2, 1.3, and 2.0 at chloride ion concentrations of 1×10^{-3}, 1×10^{-2}, and 5×10^{-2} M. Higher chloride ion concentration thus favors the production of the Pd^{III}_2 species. However, the completely electrolyzed solution was found to give no voltammetric wave in the +0.4 to −1.0 V range, indicating that subsequent chemical reactions take place after the electrochemical oxidation. The small redox peak at 0.22 V in the cyclic voltammogram is indicative of a redox process of the species produced by the subsequent chemical reactions for which further investigation is necessary to elucidate the mechanism.

Preliminary experiments showed that the bulk electrochemical oxidation of **1** at −30 °C in the presence of excess chloride ion gives a yellow-green solution that shows only a reduction wave at 0.13 V (= the oxidation potential for $[Pd_2(pyt)_4]$) in stirred-solution voltammetry. This indicates that the generated Pd^{III}_2 species remains intact at low temperature for at least the 30 min required for the measurement. However, the chemical oxidation of $[Pd_2(pyt)_4]$ with Cl_2 at −30 °C in the presence of excess chloride ion gave brown product(s), the UV–visible spectrum of which is different from that of the electrogenerated product. The differences between the chemical and electrochemical oxidation products are still under investigation.

Acknowledgment. This work was supported by a Grant-in-Aid for Scientific Research (No. 62470042) from the Ministry of Education, Science, and Culture of Japan. We are indebted to the Crystallographic Research Center of Osaka University for computation.

Supplementary Material Available: Listings of thermal parameters (Tables SIA–SIC) and full lists of bond lengths and bond angles (Tables SIIA–SIIC) (6 pages); tables of calculated and observed structure factors (8 pages). Ordering information is given on any current masthead page.

(21) The ΔE_p with iR compensation was 39 mV for Cl^- ($\Delta E_p(Fc^{+/0})$ = 61 mV).

(22) Further confirmation was made by measuring the peak current function, $i_p/v^{1/2}c^*$ (=$(2.69 \times 10^5)n^{3/2}AD_0^{1/2}$ at 25 °C: Bard, A. J.; Faulkner, L. R. *Electrochemical Methods*; John Wiley and Sons, New York, 1980; p 218). The functions were 30 and 89 μA $s^{1/2}$ $V^{-1/2}$ mM^{-1} for $[Pd_2(pyt)_4]$ in the absence (n = 1) and presence of chloride ion (0.01 M), the latter value being close to $2^{3/2} \times 30$ (=$n^{3/2} \times 30$).